Multimessenger constraints on outflows from neutron star mergers

A thesis submitted

in partial fulfillment for the award of the degree of

Master of Science

in

Astronomy and Astrophysics

by

B.S.Bharath Saiguhan

Department of Earth and Space Sciences
Indian Institute of Space Science and Technology
Thiruvananthapuram, India

May 21, 2021

Certificate

This is to certify that the thesis titled ***Multimessenger constraints on outflows from neutron star mergers*** submitted by **B.S.Bharath Saiguhan**, to the Indian Institute of Space Science and Technology, Thiruvananthapuram, in partial fulfillment for the award of the degree of **Master of Science** in **Astronomy and Astrophysics** is a bona fide record of the original work carried out by him/her under my supervision. The contents of this thesis, in full or in parts, have not been submitted to any other Institute or University for the award of any degree or diploma.

Dr. Resmi Lekshmi
Designation

Name of Department Head
Designation

Place: Thiruvananthapuram
Date: May 21, 2021

Declaration

I declare that this thesis titled ***Multimessenger constraints on outflows from neutron star mergers*** submitted in partial fulfillment for the award of the degree of **Master of Science** in **Astronomy and Astrophysics** is a record of the original work carried out by me under the supervision of **Dr. Resmi Lekshmi**, and has not formed the basis for the award of any degree, diploma, associateship, fellowship, or other titles in this or any other Institution or University of higher learning. In keeping with the ethical practice in reporting scientific information, due acknowledgments have been made wherever the findings of others have been cited.

Place: Thiruvananthapuram
Date: May 21, 2021

B.S.Bharath Saiguhan
(SC16B123)

This thesis is dedicated to ...

Acknowledgements

I acknowledge ...

B.S.Bharath Saiguhan

Abstract

Abstract here.

Contents

List of Figures

List of Tables

List of Algorithms

Abbreviations

SGRB Short Gamma-Ray Burst

Nomenclature

m	Mass of the object
c	Velocity of light

Chapter 1

Introduction

1.1 Outflows from BNS Mergers

Due to the joint electromagnetic and gravitational wave detection of the binary neutron star merger event GW1701817 (see B. Abbott et al. 2017), there has been renewed interest in SGRBs. Specifically, this detection gives credence to the claim that the central engines of SGRBs are binary neutron star mergers (see Narayan, Paczynski, and Piran 1992). However, there are other aspects of the process that are not as clear. Specifically, several aspects of GW170817 have not been completely explained. The main concerns are as follows Lazzati 2020:

- The outflow of GRB170817A was lower in energy than a typical cosmological SGRB, by a factor of $10^4 - 10^5$, even though the event was one of the closest GW events recorded, at a distance of $\sim$ 40 Mpc. This could be due to two factors :
  - The structured jet was off-axis with respect to the observer.
  - The internal engine powering this SGRB was intrinsically less energetic, and differs from the one observed in other typical SGRBs.
- A clear consensus has not been reached on how the gamma-ray prompt emission was produced. The uncertainty partly comes from the fact that the various delays involved before the prompt emission is observed are not accurately constrained. Models which have been considered include :
  - The structured outflow model, characterised by functions for the Lorentz factor and the energy per unit solid angle, both of which vary with the

angle made with the polar jet axis (θ). This model produces detectable signals even at moderately large off-axis angles.

– The shock breakout model, wherein the leading edge of the wind emits the prompt emission as it breaks out of the cocoon of nuclear matter ejected before the jet was launched. This model has been shown to explain the energetics and spectrum of the prompt emission, although it does require a setup in which the wind is fast enough so that it can reach a large enough distance at breakout.

More light can be shed on these questions by observing more such SGRBs, using both the gravitational wave (GW) and electromagnetic (EM) windows. However, the possibility of joint detections are slim, due to the fact that the EM observations are highly dependent on the viewing angle of the system with respect to the observer (due to relativistic beaming), whereas GW signal amplitudes depend on the distance to the event (see Saleem 2020).
Given that this is the case, it would be expedient to look for constraints on the structure parameters of various models. Furthermore, it would be useful to develop models which are resilient to non-detections, and can produce constraints on the parameters using even upper limits on the flux/fluence observed by the various EM follow-up satellites, such as INTEGRAL, Fermi or Swift.

1.1.1 Modelling outflows from BNS Mergers

As mentioned before, the electromagnetic follow-up of the binary neutron star merger event GW170817 helped measure the various time delays between the time of the GW signal trigger (which roughly is the merger time itself) and the time the gamma-ray signals were picked up. This time delay is denoted $\Delta t_{GW-\gamma}$, and was around 1.75 seconds for this event. The components which make up this delay are as follows Lazzati 2020:

- **Engine Delay** – this is the delay due to a transition mechanism in the central engine which powers the jet (such as a metastable, fast spinning neutron star collapsing into a black hole when its rotation period increases; this process can take years) or due to the time elapsed in amplifying the magnetic field to a

value large enough for jet launching (this process is significantly faster, taking only seconds). This is denoted by Δt_{eng}.

- **Wind Delay** – this is simply a delay in the launching of a non-relativistic wind due to the neutron-rich matter from the progenitor(s) being tidally shredded. For this reason, it can be *negative* as well, since the tidal shredding can occur before the merger itself. This is denoted as Δt_{wind}.

- **Breakout Delay** – if the wind is ejected before the jet, then the latter will have to propagate through the former. This happens at a sub-relativistic speed, whereas the GW signal travels at a relativistic speed. The delay due to this crossing is the breakout delay, and is denoted Δt_{bo}. During this time, jet-wind interactions cause the development of a structured outflow that maintains a bright core but also has energetic wings at large polar angles.

- **Photospheric Delay** – once the jet has crossed the wind, it still needs to propagate out to the photospheric radius, where the outflow becomes transparent and the prompt gamma-ray emission is radiated. The delay from the breakout radius to the photospheric radius is Δt_{ph}. This is given by (for GW170817):

$$\Delta t_{ph} \sim \frac{R_{ph}}{c\Gamma^2} = 1.4 \frac{R_{ph}}{2 \times 10^{12}\ \mathrm{cm}} \left(\frac{7}{\Gamma}\right)^2\ \mathrm{s} \tag{1.1}$$

- **Dissipation Delay** – this is a requirement in some models, such as the internal shock synchrotron model, wherein the outflow needs to travel to the internal shock radius before the bulk energy of the flow is dissipated and turned into radiation. The time required to get to this point after crossing the photospheric radius is the dissipation delay, denoted Δt_{γ}

Several attempts to constrain the various time delay components have been made. However, except for relative comparisons, no conclusions have been arrived upon. For example, one can only say that the photospheric delay is the major component out of all the delays, and that wind delay (if non-zero) has to be lesser than the jet delay, so that the jet catches up to the wind and the jet-wind interaction generates the structured outflow. Fig. **??** summarises these delays in the broader context.

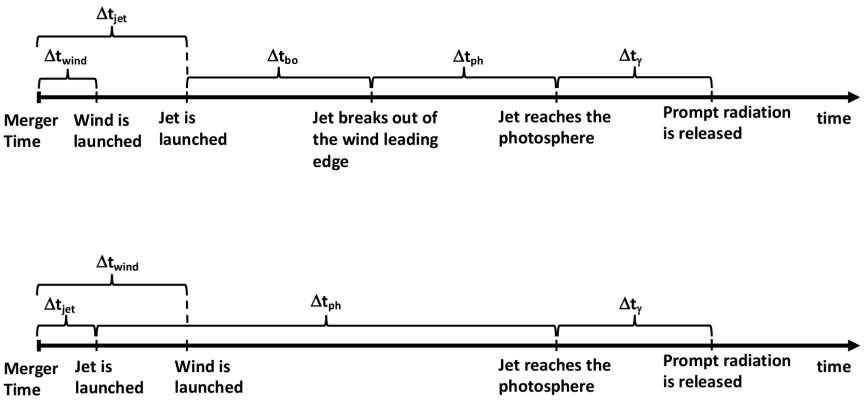

Figure 1.1: Two possible scenarios for the relative positioning of the delays in time, which contribute to $\Delta t_{GW-\gamma}$. Owing to the requirement of a structured outflow, GW170817 possibly follows the top timeline. The relative contributions of the various delays are debated, but it is agreed that $\Delta t_{wind} < \Delta t_{jet} \ll 1$ s, $\Delta t_{bo} \ll 1$ s, $\Delta t_{\gamma} \sim 0$ and $\Delta t_{ph} \sim \Delta t_{GW-\gamma}$.

Due to the uncertainties in the delay terms, several models for the jet can explain the energetics and observed structure. Numerical simulations are also unequivocal about their favouring of one model over the other (see Shibata and Hotokezaka 2019). Some models try to explain the *apparent* structure of the jet, which are the observables seen by a particular observer at a particular viewing angle. Other models are used to explain the *intrinsic* structure, such as the polar angle variation of the bulk Lorentz factor and the energy across the solid angle, in the jet co-moving frame. See Salafia et al. 2015 for a detailed discussion of the differences between the two structures. Some of the models considered are described below (see also Figs. **??** and **??**):

- Top-hat – This model, as used in M. Saleem et al. 2020, assumes that the bulk Lorentz and energy functions drop to zero beyond some cutoff angle, θ_j. Below this threshold, the functions are at their respective on-axis values.

- Gaussian – This model is widely used, in some contexts to explain the apparent jet structure (by Hayes et al. 2020), and in others the intrinsic jet structure (by M. Saleem et al. 2020). The former is simply given by $y_{GJ}(\theta) = e^{-\frac{1}{2}\left(\frac{\theta}{\theta_\sigma}\right)^2}$, since the authors consider only the apparent jet structure, as explained above and θ_σ is a structure parameter which is inferred by the authors' Bayesian inference. In the latter, as the authors consider the intrinsic jet structure, they assume

that $\Gamma\beta(\theta) = \Gamma_0\beta_0 \exp\left(-\theta^2/2\theta_c^2\right)$ and that $\epsilon(\theta) \propto \exp(-\theta^2/\theta_c^2)$[1], and derive the observed properties (see below).

- Power Law – This model is used by Hayes et al. 2020 to explain the apparent structure of the jet, assuming that any variation in the energy is simply because of relativistic beaming and the jet being viewed off-axis. It is given using the shape function $y(\theta)$ (which is multiplied with the on-axis isotropic equivalent energy $E_{iso,0}$ to give $E_{iso}(\theta)$[2]):

$$y(\theta) = \begin{cases} 1, & 0 \leq \theta \leq \theta_c, \\ (\theta/\theta_c)^{-2}, & \theta_c < \theta \leq \theta, \\ 0, & \theta_j < \theta \end{cases} \tag{1.2}$$

  Here θ_c and θ_j are simply structure parameters, inferred using Bayesian methods.

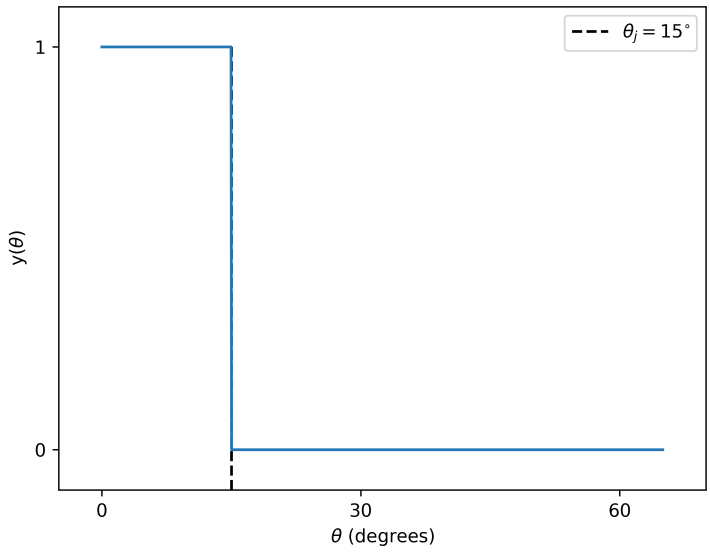

Figure 1.2: Functional form of the tophat jet structure model, as considered in M. Saleem et al. 2020. The dashed line denotes the jet angle $\theta_j = 15°$.

[1]This is the normalised energy profile function. The normalisation constant is estimated by the condition $2\pi \int d(\cos\theta)\epsilon(\theta) = E_{tot.,\gamma}$, where $E_{tot.,\gamma}$ is the total energy in gamma-rays.

[2]Using the equation $E_{iso}(\theta_v) = E_{iso,0} \cdot y(\theta_v)$

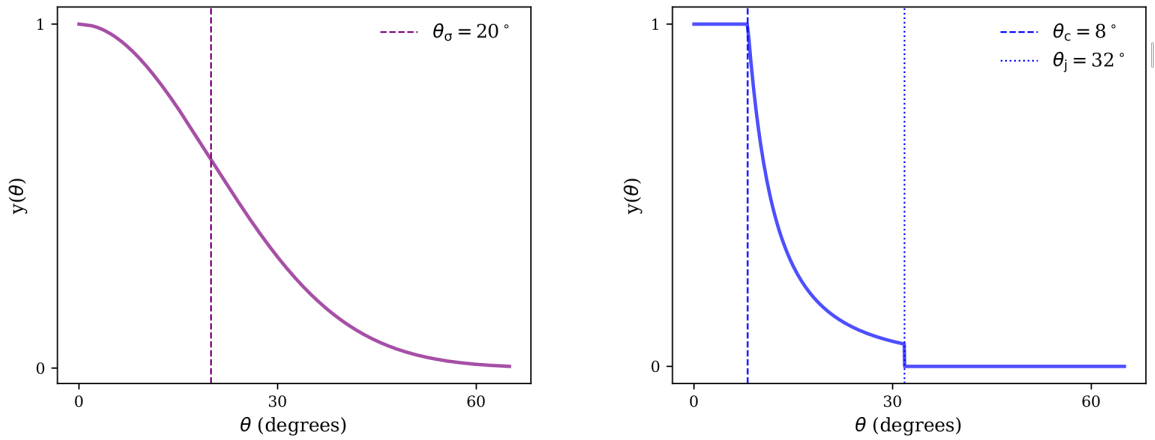

Figure 1.3: Functional forms of the jet structure models, as considered by Hayes et al. 2020. (Left) The gaussian jet structure with a width $\theta_\sigma = 20°$, also marked by the dashed line. (Right) The power-law structure with a core angle $\theta_c = 8°$ and a jet angle $\theta_j = 32°$.

In order to compute the observed structure given the intrinsic structure, following Granot et al. 2002 we start off by considering the emission profile of a point source moving at some angle with the observer, essentially rendering this scenario off-axis. This will affect the prompt jet emission, as well as the initial afterglow, and so warrants careful analysis. Now, let the initial jet opening angle be θ_0 and let the observer be at an angle θ_{obs}. In general, for a point source moving at any angle θ with respect to the observer, the observed flux is given by :

$$F_\nu = \frac{L'_{\nu'}}{4\pi d_L^2}\left(\frac{\nu}{\nu'}\right)^3 = \frac{1+z}{4\pi d_L^2}\frac{L'_{\nu'}}{\gamma^3(1-\beta\cos\theta)^3} \tag{1.3}$$

Here, $L'_{\nu'}$ and ν' are the jet comoving frame spectral luminosity and frequency, d_L is the luminosity distance, $\gamma = (1-\beta^2)^{-1/2}$ is the jet Lorentz factor. If t and ν are the observed time and frequency for an observer at θ, and t_0 and ν_0 are those for an observer on the axis, then:

$$\frac{t_0}{t} = \frac{\nu}{\nu_0} = \frac{(1-\beta)}{(1-\beta\cos\theta)} \equiv a \approx \frac{1}{(1+\gamma^2\theta^2)} \tag{1.4}$$

And finally putting Eq. **??** into Eq. **??** and expanding using a Taylor series approximation upto the leading order:

$$F_\nu(\theta_{obs}, t) = a^3 F_{\nu/a}(0, at) \tag{1.5}$$

This gives us a handle on how to relate observed off-axis quantities to the on-axis ones. Furthermore, this enables us to go from an intrinsic structure to an observed one, which is what was required.

1.2 Outflows from NSBH Mergers

The main difference in the NSBH merger pathway to SGRBs, compared to the case of BNS mergers, is that though there is theoretical and simulational support for the launching of SGRB jets from the merger of a neutron star and a black hole of appropriate mass (see for example Ruiz et al. 2020, Shibata and Hotokezaka 2019, Francois Foucart 2020), there has not been strong observational evidence for the same. In the first half of the third observing run of the LVC (also known as O3a), there have been several triggers which have been reportedly confident NSBH triggers. However, there were no counterpart EM signals picked up, which decreases the credibility of NSBH mergers as the progenitors of SGRBs.

The electromagnetic component from NSBH mergers, is largely decided based on the amount of mass left post-merger, outside the horizon of the black hole. This decides how much matter participates in the subsequent processes, which may be the rapid neutron-capture process which gives rise to the kilonova signal or the magnetic field amplification process via the Magneto-Rotational Instability (MRI) which leads to a SGRB jet.

Qualitatively, for a binary where the neutron star is treated as a test mass and the black hole's spin is aligned with the orbital angular momentum of the binary, the innermost-stable circular orbit radius r_{ISCO} scales as $r_{ISCO} \sim f(\chi_{BH})GM_{BH}/c^2$ (where f is a function ranging from 1 to 9, decreasing for increasing (prograde) spins; see Bardeen, Press, and Teukolsky 1972) and the radius at which the tidal disruption of the neutron star occurs, r_{dis} scales as $r_{dis} \sim k(M_{BH/M_{BNS}})^{1/3}R_{NS}$ (where k is a constant with a dependence on the black hole spin and the equation of state). Only requiring that $r_{dis} \gtrsim r_{ISCO}$, as a rough requirement for disruption to occur before the neutron star plunges into the black hole, leads to the conclusion that (a.) low-mass black holes (b.) larger NS radii (c.) higher prograde black hole spins favour disruption. This is seen from Fig. **??** as well. However, for actual quantitative results simulations need to be performed such the effect of the various components in the problem are correctly taken into account. As seen from the literature, wherein such general-relativistic magnetohydrodynamic simulations are carried out, the matter left

over post-merger heavily depends on (for a summary, see Fig. **??**):

- **The mass ratio of the system**. This is defined as $q = M_{BH}/M_{NS}$ so that $q > 1$ always. Fully general relativistic, magnetohydrodynamic simulations (such as Ruiz et al. 2020) show that in cases where the mass ratio is 3:1, regardless of the neutron spin, a collimated outflow is observed, whereas the same is not realised in cases where the mass ratio is 5:1 or higher.

- **The spin of the components of the system**. In geometrized units (where $G = c = 1$), these are prescribed in terms of a_{BH}/M_{BH} or a_{NS}/M_{NS}, and whether these two spins align (prograde) or are anti-aligned (retrograde) decides whether the neutron star would be tidally disrupted, and hence participate in the processes mentioned previously, or not. Via simulations, it is seen that the more the prograde spin of the neutron star, the farther out the neutron star is tidally disrupted, albeit this is only observed for the case of q = 3:1 (comparing say, Figs. **??** and **??**). Also, this leads to long tidal tails, which produces a baryon-loaded environment and thus the magnetic field of the tidally disrupted matter must overcome the baryon ram pressure to launch the jet. This process hence delays the launching of the jet.

Aside from the SGRB jet, which requires magnetic field amplification (via MRI) as well as thermal pair production (from the disk remnant) followed by the Blandford-Znajek process, there is a possibility that NSBH mergers can produce kilonovae signatures. For this, the dynamically ejected mass has to be between $10^{-4.5} - 10^{-2}(M_{NS}/1.4M_{\odot})M_{\odot}$ (see Ruiz et al. 2020 for more details), and this will lead to kilonovae potentially detectable by the Large Synoptic Survey Telescope (LSST).

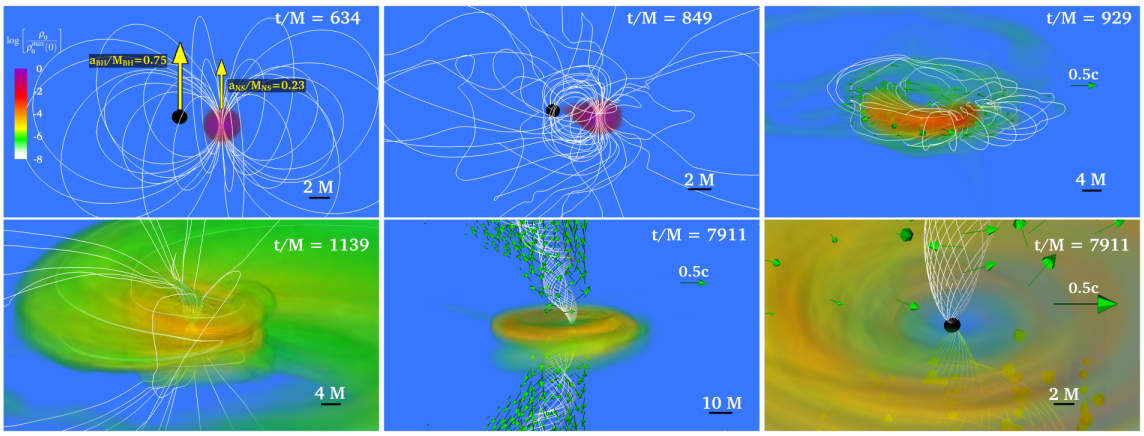

Figure 1.4: Volume rendering of the rest mass density (ρ_0) (in log scale), normalized to the NS maximum value $\rho_0 = 8.92 \times 10^{14} (1.4 M_\odot / M_{NS})^2$ g/cm^3, for particular times for a magnetized neutron star, with q = 3:1 and a prograde NS spin of 0.23. Top three panels highlight the inspiral and the tidal disruption, whereas the bottom three panels highlight the appearance of the magnetically-driven jet. White lines denote the magnetic field, arrows denote the fluid velocity and the BH's apparent horizon is the black sphere. Here M $= 2.5 \times 10^{-2} (M_{NS}/M_{1.4M_\odot})$ ms $= 7.58 (M_{NS}/M_{1.4M_\odot})$ km (in geometrized units). From Ruiz et al. 2020.

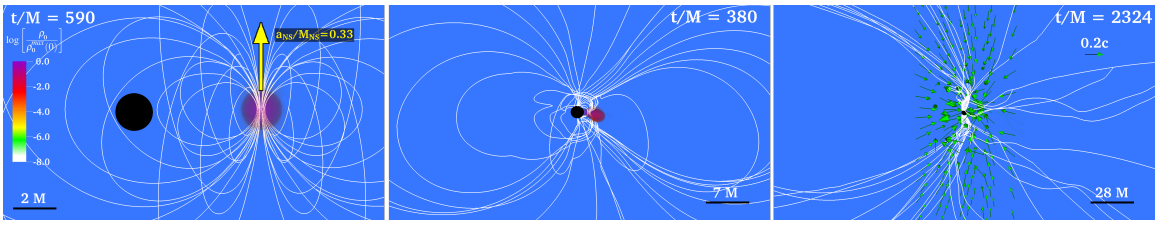

Figure 1.5: Similar to Fig. **??**, however with the NS spin being 0.33, the BH spin being 0 and q = 5:1. In this case, no strong collimation of the magnetic field is observed from the merger remnant, and so a magnetically-driven jet is also not observed. From Ruiz et al. 2020.

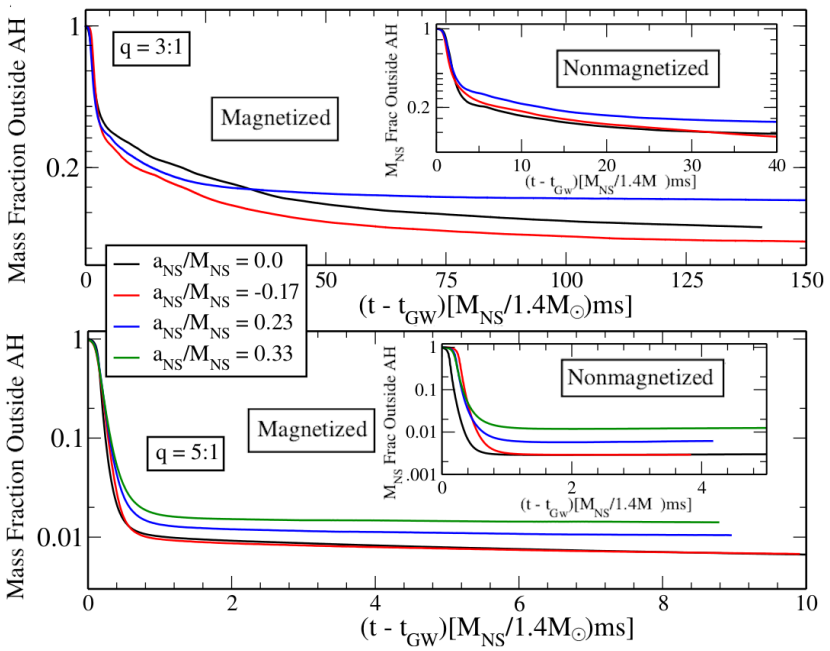

Figure 1.6: Fraction of rest-mass of the NS outside the apparent horizon of the black hole as a function of coordinate time, for the various configurations considered in Ruiz et al. 2020. The inset figures report the same for non-magnetized cases, and the coordinate time is shifted such that the merger time coincides with 0.

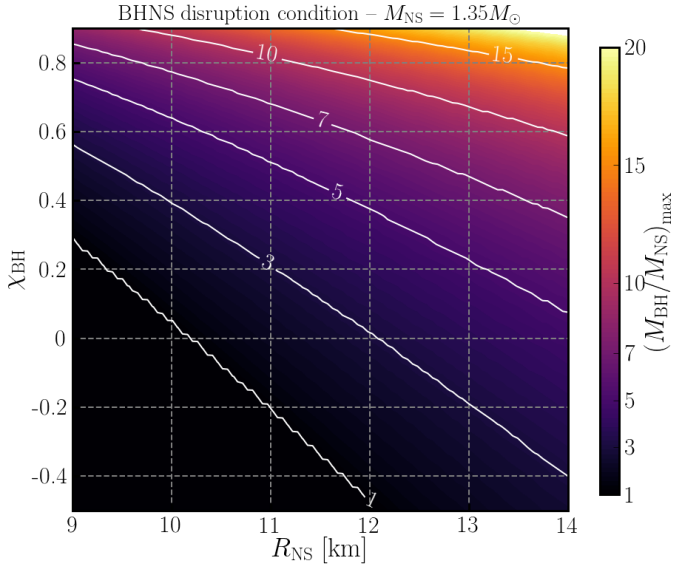

Figure 1.7: Maximum value of the mass-ratio (M_{BH}/M_{NS}) for which a NSBH system disrupts, as a function of the neutron star radius R_{NS}, and the aligned component of the dimensionless black hole spin χ_{BH}, assuming $M_{NS} = 1.35M_\odot$. Results for other neutron star masses can be obtained by rescaling considering the disruption condition at constant compaction $C_{NS} = GM_{NS}/R_{NS}c^2$. From Francois Foucart 2020.

1.2.1 Modelling outflows from NSBH Mergers

As mentioned before, the outflows from NSBH mergers depend on the amount of mass left outside the event horizon post-merger. In the work done by Francois Foucart, Hinderer, and Nissanke 2018, the authors consider a suite of 75 numerical relativity simulations of NSBH mergers over the parameter space $\mathcal{Q} \in [1, 7]$, $\chi_{BH} \in [-0.5, 0.97]$, $\mathcal{C}_{NS} \in [0.13, 0.182]$[3] and fit the results for the *remnant mass* $M_{\rm rem}$ (sometimes also denoted as $M_{\rm out}$), as a function of the binary parameters (masses, spins of the components, tidal deformability of the neutron star etc). This fit is given as follows:

$$M_{\rm out} = M_{NS}^{b} \cdot \max\left(\alpha \frac{1-2\rho}{\eta^{1/3}} - \beta \hat{R}_{\rm ISCO}\frac{\rho}{\eta} + \gamma, 0\right)^{\delta} \tag{1.6}$$

where:

- The baryonic mass of the neutron star is given by the equation

$$M_{NS}^{b} = M_{NS}\left(1 + \frac{0.6 C_{NS}}{1 + 0.5 C_{NS}}\right)$$

- The tidal deformability of the neutron star is given by Λ_{NS} and $\rho = (15\Lambda_{NS})^{-1/5}$. It is also related to the compactness of the neutron star via the C-Love relation (see Yagi and Yunes 2017):

$$C_{NS} = \sum_{k=0}^{2} a_k (\ln \Lambda_{NS})^k \tag{1.7}$$

  where $a_0 = 0.360, a_1 = -0.0335, a_2 = 0.000705$.

- η is the symmetric mass ratio, given by $\eta = \dfrac{\mathcal{Q}}{(1+\mathcal{Q})^2}$.

- $\hat{R}_{ISCO} = c^2 R_{ISCO}/GM_{BH}$ is the normalized ISCO radius for a spinning black hole, given in Bardeen, Press, and Teukolsky 1972 as :

$$\begin{aligned} &\hat{R}_{ISCO} = 3 + Z_2 - \mathrm{sgn}(\chi_{BH})\sqrt{(3-Z_1)(3+Z_1+2Z_2)} \\ &\hookrightarrow Z_1 = 1 + (1-\chi_{BH}^2)^{1/3}[(1+\chi_{BH})^{1/3} + (1-\chi_{BH})^{1/3}] \\ &\hookrightarrow Z_2 = \sqrt{3\chi_{BH}^2 + Z_1^2} \end{aligned} \tag{1.8}$$

[3]Here, $\mathcal{Q} = M_{BH}/M_{NS}$ is the mass-ratio, $\chi_{BH} = c|\mathbf{S}|/GM_{BH}^2$ is the effective spin of the black hole and $C_{NS} = GM_{NS}/R_{NS}c^2$ is the compactness of the neutron star.

- $(\alpha, \beta, \gamma, \delta) \equiv (0.308, 0.124, 0.283, 1.536)$ are the fit coefficients.

Similarly, Kawaguchi et al. 2016 fit to the results of 45 numerical relativity simulations over the parameter space $\mathcal{Q} \in [3, 7]$, $\chi_{\rm BH} \in [0, 0.90]$, $C_{\rm NS} \in [0.138, 0.180]$. This fit produces a formula for the *dynamic* mass $M_{\rm dyn}$, which is the unbound mass ejected at the time of disruption, in terms of the binary parameters. This fit is given as follows:

$$\frac{M_{dyn}}{M_{NS}^{b}} = \max\Bigg\{ a_1 Q^{n_1}(1 - 2C_{NS})C_{NS}^{-1} - a_2 Q^{n_2}\hat{R}_{ISCO}(\chi_{BH}) + a_3\left(1 - \frac{M_{NS}}{M_{NS}^{b}}\right) + a_4, 0 \Bigg\} \quad (1.9)$$

where the symbols have their usual meanings, and additionally:

$$a_1 = 4.464 \times 10^{-2} \qquad a_2 = 2.269 \times 10^{-3}$$
$$a_3 = 2.431 \qquad a_4 = -0.4159$$
$$n_1 = 0.2497 \qquad n_2 = 1.352$$

From these two quantities, we can derive the disc mass $M_{\rm disc}$ as :

$$M_{\rm disc} = \max\{M_{\rm out} - M_{\rm dyn}, 0\} \quad (1.10)$$

However, due to the fact that these two fits are derived from simulations over different regions of the input parameter space, care must be taken while applying them together. This is to ensure that $M_{\rm dyn} \leq M_{\rm out}$ always, so that the disc mass is non-negative. This validation is performed by considering the ratio $M_{\rm out}/M_{\rm dyn}$. Another constraint is imposed, which is motivated by the fact that NSBH simulations carried out by F. Foucart et al. 2019 in the near-equal mass ratio regime found an unbound component no more massive than roughly 30% of the total remnant mass (note that one expects maximal tidal disruption in this regime, given a fast spinning black hole). Thus we set:

$$M_{\rm dyn,max} = f \cdot M_{\rm rem} = 0.3 \cdot M_{\rm rem} \quad (1.11)$$

Additionally, the masses of the other wind ejecta, namely the neutrino-driven and

viscosity-driven wind ejecta, are derived from that of the disc mass:

$$\begin{aligned} M_{\rm vis} &= \xi_{\rm vis} M_{\rm disc} = 0.2 M_{\rm disc} \\ M_{\nu} &= \xi_{\nu} M_{\rm disc} = 0.01 M_{\rm disc} \end{aligned} \tag{1.12}$$

To model the SGRB jet, the procedure of Zhu et al. 2020 is followed. The kinetic energy of the jet is decided by the disc mass and the black hole spin as follows:

$$E_{\rm K,jet} = \epsilon(1 - \xi_{\rm vis} - \xi_{\nu}) M_{\rm disc} c^2 \Omega_H^2 f(\Omega_H) \tag{1.13}$$

where:

- The dimensionless angular velocity at the horizon of the black hole is given by:

$$\Omega_H = \frac{\chi_{BH}}{2(1 + \sqrt{1 + \chi_{BH}^2}} \tag{1.14}$$

- $f(\Omega_H)$ is a high-spin correction factor given by

$$f(\Omega_H) = 1 + 1.38\Omega_H^2 - 9.2\Omega_H^4$$

- ϵ is a fudge factor which depends on the large-scale geometry of the magnetic field, disc aspect ratio and the ratio of the magnetic field energy density to disc pressure at saturation.
  In order to set it to a definite value, it is noted that the maximum disc mass cannot exceed the total NS baryonic mass i.e. $M_{\rm disc} \lesssim 2M_{\odot}$. Also, the spin-dependent factor $\Omega_H^2 f(\Omega_H)$ cannot exceed 0.2 (since $\chi_{BH} \in [-1, 1]$). Furthermore, the most energetic of SGRBs has had a $E_{\gamma,\rm iso} \sim 7.4 \times 10^{52}$ erg, and if one assumes a 10% conversion efficiency of kinetic to gamma-ray energy alongwith a typical jet opening angle of 5°, this corresponds to a kinetic energy of $E_{\rm K,jet} \sim 3 \times 10^{52}$ erg.
  Based on this, once can calculate $\boxed{\epsilon \approx 0.015}$.

Using this we can define the structure of the SGRB jet, given by the following equations:

$$\frac{dE(\theta)}{d\Omega} = \frac{E_{\rm k,jet}}{\pi \theta_{\rm c,E}^2} e^{-(\theta/\theta_{\rm c,E})^2} \tag{1.15}$$

$$\Gamma(\theta) = (\Gamma_c - 1)e^{-(\theta/\theta_{\rm c,E})^2} + 1 \tag{1.16}$$

$$E_{\rm iso}(\theta_v) = \eta \int \frac{\delta^3}{\Gamma} \frac{dE}{d\Omega} d\Omega \tag{1.17}$$

where:

- $\Gamma_c = 100, \theta_{\rm c,E} = 0.1, \theta_{\rm c,\Gamma} = 0.2$. See Salafia et al. 2015 and Barbieri et al. 2019.
- η is the conversion efficiency of gamma-ray energy to kinetic energy, which is traditionally taken to be 10%.
- δ is the Doppler factor, given by

  $$\delta = \frac{1}{\Gamma[1 - \beta \cos \alpha_v]}$$

  where α_v is the angle between the jet element at (θ, ϕ) and the observer's direction.

1.3 NS mergers in GW regime

Consider any astrophysical source emitting gravitational waves, which come in two polarizations, namely the *plus* $h_+(t; \mathbf{\Theta}_{GW})$ and the *cross* $h_\times(t; \mathbf{\Theta}_{GW})$ polarizations. Here $\mathbf{\Theta}_{GW}$ is the parameter vector, and is typically $\{m_1, m_2, \chi_1, \chi_2, D_L, \iota, t_c, \phi_c\}$ which are the component masses, component spins, the binary's luminosity distance, the inclination angle of the orbital plane with respect to the line of sight, and two constants of integration: the time and phase of coalescence.
A detector's response is recorded as the GW strain such waveforms produce, but in the frequency domain and so the input waveforms are Fourier transformed before processing. Also the detector's antenna patterns (sensitivity as a function of the source location on the sky) and location phase factor (effect of the earth's rotation) play a role in the response. Thus, the detector response to these gravitational waves is of the form:

$$H(f; \mathbf{\Theta}) = F_{lp}(f; \alpha, \delta) \cdot [H_+(f; \mathbf{\Theta}_{GW}) F_+(f; \alpha, \delta, \psi) + H_\times(f; \mathbf{\Theta}_{GW}) F_\times(f; \alpha, \delta, \psi)] \tag{1.18}$$

where F_{lp} is the location phase factor as a function of the frequency and the source RA and declination, $H_{+/\times}$ are the frequency domain waveforms, and $F_{+/\times}$ are the detector antenna patterns for each polarization. Also $\mathbf{\Theta} = \{\mathbf{\Theta}_{GW}, \alpha, \delta, \psi\}$.
The sensitivity of a detector is given by the detector's noise $n(t)$ and its autocorrelation $\kappa = \overline{n(t_1)n(t_2)}$. Usually, the noise is assumed to be stationary, zero-mean and Gaussian. Thus, one can define the one-sided power spectral density $S_n(f)$ as the Fourier transform of the autocorrelation.
From this, one can define the 'overlap' between two GW signals (for eg.: the detector responses for two different waveforms) using the noise-weighted scalar product:

$$\langle H, G\rangle = 2\int_0^\infty \frac{H(f)G^*(f) + H^*(f)G(f)}{S_n(f)}df \tag{1.19}$$

And using this definition of the scalar product, the signal-to-noise ratio is defined as :

$$\rho^2 = \langle H, H\rangle = 4\int_0^\infty \frac{|H(f)|^2}{S_n(f)}df \tag{1.20}$$

Now, since the noise $n(t) = s(t) - h(t)$ is assumed to a zero-mean Gaussian, its Fourier transform also behaves the same way, and thus the probability of noise can be written down as :

$$p(\mathbf{\Theta}) = p^0(\mathbf{\Theta})e^{-\frac{1}{2}\langle S-H(\mathbf{\Theta}), S-H(\mathbf{\Theta})\rangle} \tag{1.21}$$

where p^0 is the prior on the parameter vector of the detector response. Assuming that an event signal S has a high SNR, the value of $\mathbf{\Theta}$ at peak probability is a good estimate of the true value $\mathbf{\Theta}^*$. Additionally peak probability occurs when the exponential $E = \langle S - H, S - H\rangle$ is the largest. Expanding it around the maximum value:

$$E(\mathbf{\Theta}) = E(\mathbf{\Theta}^*) + \frac{1}{2}\frac{\partial^2 E(\mathbf{\Theta})}{\partial\Theta_i\partial\Theta_j}\bigg|_{\mathbf{\Theta}=\mathbf{\Theta}^*}\Delta\Theta_i\Delta\Theta_j + \cdots \tag{1.22}$$

where $\Delta\Theta_i = \Theta_i - \Theta_i^*$. The Hessian given by:

$$\frac{\partial^2 E(\mathbf{\Theta})}{\partial\Theta_i\partial\Theta_j} = 2\langle\partial_{\Theta_i}H(\mathbf{\Theta}), \partial_{\Theta_j}H(\mathbf{\Theta})\rangle + \langle\partial_{\Theta_i}\partial_{\Theta_j}H(\mathbf{\Theta}), N\rangle \tag{1.23}$$

can be simplified for large SNR, where second-order differentials become negligible. This leads to the definition of the Fisher Information Matrix Γ:

$$\Gamma_{ij} = \langle\partial_{\Theta_i}H(\mathbf{\Theta}), \partial_{\Theta_j}H(\mathbf{\Theta})\rangle \tag{1.24}$$

And hence, Eqn. **??** becomes:

$$p(\mathbf{\Theta}) \sim \exp\left(-\frac{1}{2}\Gamma_{ij}\Delta\Theta_i\Delta\Theta_j\right) \tag{1.25}$$

which implies that the assumption of Gaussian noise helps associate the FIM to the inverse of the covariance matrix $\Sigma \equiv \Gamma^{-1}$. This also means that the diagonal and off-diagonal elements of Γ^{-1} denote the variances and covariances of the parameters, respectively, with 1σ estimates of the error are given as $\sigma_{\Theta_i} = \sqrt{\Sigma_{ii}}$.
This Fisher Information Matrix (FIM) formalism[4] is a method of rapid GW data analysis, which approaches the accuracy of traditional Bayesian parameter estimation for events with large SNR.
GWBENCH (see Borhanian 2020) is a GW benchmarking tool, which can compute the Fisher matrix for a particular NS merger, given the network configuration and binary parameters. In this way, it enables rapid calculations to benchmark detector upgrades as well as forecast the confidence with which parameters may be estimated for the NS mergers in question.

1.4 Summary

NS mergers can present an ideal testing environment for physical theories under extreme gravity, and by observing them in both the EM and GW windows, current theories can be better understood and refined. Several questions also remain about the exact mechanisms which power the outflows from these NS mergers.
In this report, we focus mainly on SGRB jets from NSBH mergers and perform population synthesis studies to infer the conditions for and implications of observing a SGRB jet from NSBH mergers.

[4]Sometimes also referred to as the Fisher Information Formalism (FIF), in which case the Fisher information is not a matrix but is instead the variance of the partial derivative with respect to the parameter vector, of the natural logarithm of the likelihood function for the random variable whose parameters are to be estimated.

Chapter 2
Population Synthesis

2.1 Summary

Chapter 3
Population Analysis

3.1 Summary

Chapter 4

NS Merger Candidates in GWTC-2

4.1 About GWTC-2

The first half of the third observing run (O3a) of the LVC started on the 1st of April 2019, and went on till 30th of September, 2019. Following this, instrumental upgrades were made during the month of October and the second half of the third observing run (O3b) was started on the 1st of November. Due to the global pandemic, the observing run had to be prematurely suspended on 30th of March, 2020.
Starting with O3, alerts were distributed via the public alerts section of Gravitational-wave Candidate Event Database (GRACE-DB). If triggers were registered that passed the detection threshold of the LVC network during observational runs, online parameter estimation was done using the raw GW data, and low latency estimates of the rough sky position, component masses and luminosity distance was made available for observers in the EM regime. This allowed for rapid follow-up in various bands of the electromagnetic spectrum, and these observations were reported and cross-verified using NASA's GRB Coordinates Network (GCN). Using the circulars reported in the GCN for NSBH/BNS events of interest, along with the low-latency information from GRACE-DB, O3a's non-BBH candidate events have been collected in table **??**
More detailed analysis of these events in the months following has led to at least 53 events in the third observing run alone. These can be classified as:

- 37 Binary Black Hole (BBH) merger candidates.
- 7 BNS merger candidates. Of these, only 1 corresponds to O3a, which is the event GW190425 discussed in the chapter **sec:190425**.
- 4 events in the mass gap, which are events with compact objects with masses of 3-5 $M_{\odot}$.

- 5 NSBH merger candidates. Of these, only 1 has been confirmed officially, which is the event GW190814.

Of these, 26 events were officially confirmed and 13 new events were reported for the first time in R. Abbott et al. 2020, and it is from there that the posterior distributions of the various parameters (such as inclination angle ι, luminosity distance D_L etc) are used for further analysis. Note also that there are several marginal events that have been reported, in that they have non-negligible probability distributed between two classifications. For example, the event GW190426_152155 has significant probability split between it being a terrestrial event (58 %) and a NSBH/BNS/Mass Gap event (cumulatively 42%). Without a significant EM counterpart, this event cannot be confidently placed in either of the classes, and thus warrants further analysis. This is the subject of chapter **sec:190426**.

GRACE-DB Superevent ID	$\mathcal{P}$**(BBH)**	$\mathcal{P}$**(BNS)**	$\mathcal{P}$**(MassGap)**	$\mathcal{P}$**(NSBH)**	$\mathcal{P}$**(Terr)**
S190426c	0	24	12	6	58
S190910h	0	61	0	0	39
S200213t	0	63	0	0	37
S191213g	0	77	0	0	23
S190901ap	0	86	0	0	14
S190425z	0	**>99**	0	0	0
S190930s	0	0	95	0	5
S190923y	0	0	0	68	32
S190930t	0	0	0	74	26
S191205ah	0	0	0	93	7
S190910d	0	0	0	98	2
S190814bv	0	0	0	**>99**	0

Table 4.1: List of candidate merger events and the probability of classification (reported in %) for each non-BBH event reported during O3a. Here the GRACE-DB superevent ID is used (instead of the GWTC-2 event ID), since for a particular GW event, the superevent collects both the EM followup as well as GW trigger information within GRACE-DB. The probabilities are assigned using the process described in Kapadia et al. 2020, and are reported in GRACE-DB. The events underlined are discussed in more detail in later chapters.

UID	FAR	D_L (Mpc)	Error in D_L (Mpc)
S190426c	1 per 1.6276 yr	377	100
S190910h	1.1312 per yr	230	88
S200213t	1 per 1.7934 yr	201	80
S191213g	1.1197 per yr	201	81
S190901ap	1 per 4.5093 yr	241	79
S190425z	1 per 69834 yr	158	43
S190930s	1 per 10.534 yr	709	191
S190923y	1.5094 per yr	438	133
S190930t	1 per 2.0536 yr	108	38
S191205ah	1 per 2.5383 years	385	164
S190910d	1 per 8.5248 years	606	197
S190814bv	1 per 1.559e+25 years	241	26

Table 4.2: List of candidate merger events and the probability of classification for each non-BBH event reported during O3a. FAR refers to the False Alarm Rate (in number of events per year or equivalently in Hz^{-1}), and D_L is the luminosity distance. Both these values are those reported in GRACE-DB corresponding to each event. The events underlined are discussed in more detail in later chapters.

UID	FERMI-LAT	FERMI-GBM	SWIFT/BAT	INTEGRAL
S190426c	24342	24248	24255	24242
S190910h	25742	25714	25718	25709
S200213t	27062	27056	27058	27050
S191213g	26412	26409	26410	26401
S190901ap	25625	25610	25617	25605
S190425z	24266	24185	24184, 24296	24169, 24170 24178, 24181
S190930s	25895	25886	25889	25872
S190923y	25834	25823	25846	25815, 25825
S190930t	25898	25887	25888	25880
S191205ah	26363	26359	26365	26531
S190910d	25717	25699	25704	25698
S190814bv	25385	25326	25341	25323

Table 4.3: List of candidate merger events and the probability of classification for each non-BBH event reported during O3a. Here the GCN Circular number reporting the findings of the particular instrument in the column heading is reported, corresponding to each event. The events underlined are discussed in more detail in later chapters. GCNs marked with red should be ignored during analysis since they correspond to times when the respective instruments were in the South Atlantic Anomaly (SAA).

4.2 Summary

Chapter 5

Results and Discussion

5.1 Summary

References

Abbott, B. P. et al. (Oct. 2017). "GW170817: Observation of Gravitational Waves from a Binary Neutron Star Inspiral". In: *Physical Review Letters* 119.16. DOI: 10.1103/physrevlett.119.161101. URL: https://doi.org/10.1103/physrevlett.119.161101.

Abbott, R. et al. (Oct. 2020). "GWTC-2: Compact Binary Coalescences Observed by LIGO and Virgo During the First Half of the Third Observing Run". In: *arXiv e-prints*, arXiv:2010.14527, arXiv:2010.14527. arXiv: 2010.14527 [gr-qc].

Barbieri, C. et al. (May 2019). "Light-curve models of black hole – neutron star mergers: steps towards a multi-messenger parameter estimation". In: *Astronomy & Astrophysics* 625, A152. DOI: 10.1051/0004-6361/201935443. URL: https://doi.org/10.1051/0004-6361/201935443.

Bardeen, James M., William H. Press, and Saul A. Teukolsky (Dec. 1972). "Rotating Black Holes: Locally Nonrotating Frames, Energy Extraction, and Scalar Synchrotron Radiation". In: *The Astrophysical Journal* 178, p. 347. DOI: 10.1086/151796. URL: https://doi.org/10.1086/151796.

Borhanian, Ssohrab (Oct. 2020). "gwbench: a novel Fisher information package for gravitational-wave benchmarking". In: *arXiv e-prints*, arXiv:2010.15202, arXiv:2010.15202. arXiv: 2010.15202 [gr-qc].

Foucart, F. et al. (May 2019). "Numerical simulations of neutron star-black hole binaries in the near-equal-mass regime". In: *Physical Review D* 99.10. DOI: 10.1103/physrevd.99.103025. URL: https://doi.org/10.1103/physrevd.99.103025.

Foucart, Francois (July 2020). "A Brief Overview of Black Hole-Neutron Star Mergers". In: *Frontiers in Astronomy and Space Sciences* 7. DOI: 10.3389/fspas.2020.00046. URL: https://doi.org/10.3389/fspas.2020.00046.

Foucart, Francois, Tanja Hinderer, and Samaya Nissanke (Oct. 2018). "Remnant baryon mass in neutron star-black hole mergers: Predictions for binary neutron

star mimickers and rapidly spinning black holes". In: *Physical Review D* 98.8. DOI: 10.1103/physrevd.98.081501. URL: https://doi.org/10.1103/physrevd.98.081501.

Granot, Jonathan et al. (May 2002). "Off-Axis Afterglow Emission from Jetted Gamma-Ray Bursts". In: *The Astrophysical Journal* 570.2, pp. L61–L64. DOI: 10.1086/340991. URL: https://doi.org/10.1086/340991.

Hayes, Fergus et al. (Mar. 2020). "Comparing Short Gamma-Ray Burst Jet Structure Models". In: *The Astrophysical Journal* 891.2, p. 124. DOI: 10.3847/1538-4357/ab72fc. URL: https://doi.org/10.3847/1538-4357/ab72fc.

Kapadia, Shasvath J et al. (Jan. 2020). "A self-consistent method to estimate the rate of compact binary coalescences with a Poisson mixture model". In: *Classical and Quantum Gravity* 37.4, p. 045007. DOI: 10.1088/1361-6382/ab5f2d. URL: https://doi.org/10.1088/1361-6382/ab5f2d.

Kawaguchi, Kyohei et al. (June 2016). "Models of Kilonova/Macronova Emission from Black Hole–Neutron Star Mergers". In: *The Astrophysical Journal* 825.1, p. 52. DOI: 10.3847/0004-637x/825/1/52. URL: https://doi.org/10.3847/0004-637x/825/1/52.

Lazzati, Davide (Nov. 2020). "Short Duration Gamma-Ray Bursts and Their Outflows in Light of GW170817". In: *Frontiers in Astronomy and Space Sciences* 7. DOI: 10.3389/fspas.2020.578849. URL: https://doi.org/10.3389/fspas.2020.578849.

Narayan, Ramesh, Bohdan Paczynski, and Tsvi Piran (Aug. 1992). "Gamma-ray bursts as the death throes of massive binary stars". In: *The Astrophysical Journal* 395, p. L83. DOI: 10.1086/186493. URL: https://doi.org/10.1086/186493.

Ruiz, Milton et al. (Dec. 2020). "Black hole-neutron star coalescence: Effects of the neutron star spin on jet launching and dynamical ejecta mass". In: *Physical Review D* 102.12. DOI: 10.1103/physrevd.102.124077. URL: https://doi.org/10.1103/physrevd.102.124077.

Salafia, O. S. et al. (May 2015). "Structure of gamma-ray burst jets: intrinsic versus apparent properties". In: *Monthly Notices of the Royal Astronomical Society* 450.4, pp. 3549–3558. DOI: 10.1093/mnras/stv766. URL: https://doi.org/10.1093/mnras/stv766.

Saleem, M (Jan. 2020). "Prospects of joint detections of neutron star mergers and short GRBs with Gaussian structured jets". In: *Monthly Notices of the Royal*

Astronomical Society 493.2, pp. 1633–1639. DOI: 10.1093/mnras/staa303. URL: https://doi.org/10.1093/mnras/staa303.

Saleem, M. et al. (Mar. 2020). "On the Energetics of a Possible Relativistic Jet Associated with the Binary Neutron Star Merger Candidate S190425z". In: *The Astrophysical Journal* 891.2, p. 130. DOI: 10.3847/1538-4357/ab6731. URL: https://doi.org/10.3847/1538-4357/ab6731.

Shibata, Masaru and Kenta Hotokezaka (Oct. 2019). "Merger and Mass Ejection of Neutron Star Binaries". In: *Annual Review of Nuclear and Particle Science* 69.1, pp. 41–64. DOI: 10.1146/annurev-nucl-101918-023625. URL: https://doi.org/10.1146/annurev-nucl-101918-023625.

Yagi, Kent and Nicolás Yunes (Apr. 2017). "Approximate universal relations for neutron stars and quark stars". In: *Physics Reports* 681, pp. 1–72. DOI: 10.1016/j.physrep.2017.03.002. URL: https://doi.org/10.1016/j.physrep.2017.03.002.

Zhu, Jin-Ping et al. (June 2020). "Kilonova Emission from Black Hole–Neutron Star Mergers. I. Viewing-angle-dependent Lightcurves". In: *The Astrophysical Journal* 897.1, p. 20. DOI: 10.3847/1538-4357/ab93bf. URL: https://doi.org/10.3847/1538-4357/ab93bf.